Supporting Information

Unveiling the capacitive energy storage of linear CTAB or tetrahedral TBAB organic-molecular intercalated MoS_2

Xin Wang [a,c], Mingzhu Ma [a], Weixin Wang [a], Can Tang [a], Zhongliao Wang [a,c], Jie Ru[c] Han Li [a,c], Bing Li [a], Yongxing Zhang [a,c *], Xuebin Zhu [b]*

[a] Anhui Province Key Laboratory of Pollutant Sensitive Materials and Environmental Remediation, School of Physics and Electronic Information, Huaibei Normal University, Huaibei 235000, P. R. China.

[b] Key Laboratory of Materials Physics, Institute of Solid State Physics, Chinese Academy of Sciences, Hefei 230031, People's Republic of China.

[c] Anhui Province Industrial Generic Technology Research Center for Alumics Materials, Huaibei Normal University, Huaibei, Anhui 235000, P. R. China.

***Corresponding authors.**

E-mail address: wkangxin@163.com **(X. Wang);**

zyx07157@mail.ustc.edu.cn **(Y. X. Zhang)**

Experimental Methods

Material preparation：

Synthesis of anode material 2H-MoS_2: the precursors are $(NH_4)_6Mo_7O_{24}\cdot 4H_2O$ (CAS number:12054-85-2) and CH_4N_2S (CAS number:6256-6) (the reagents used are purchased from the Reagent Network of Sinopharm Group and have not been further treated before use). Dissolve 1.4484g $(NH_4)_6Mo_7O_{24}\cdot 4H_2O$ and 2.8418g CH_4N_2S in a beaker containing 60 ml of deionized water, and stir with a magnetic stirrer for 30 minutes to form a uniform solution. Then transfer the solution to the reactor lining made of PTFE and place it in the stainless-steel reactor shell. The hydrothermal reactor was placed in a constant temperature blast drying oven and removed after 18 h of reaction at 210 ℃. The precipitate was collected by centrifugation and washed several times with deionized water and absolute ethanol, and the last wash precipitate was collected and dried in a vacuum drying oven for 24 h to obtain a 2H-Mo_2 powder sample.

Synthesis of anode material 2H-MoS_2-TBAB: the precursors are $(NH_4)_6Mo_7O_{24}\cdot 4H_2O$ (CAS number:12054-85-2)、CH_4N_2S (CAS number:6256-6) and Tetrabutylammonium bromide (TBAB) (CAS number:1643-19-2) (the reagents used are purchased from the Reagent Network of Sinopharm Group and have not been further treated before use). Dissolve 1.4484g $(NH_4)_6Mo_7O_{24}\cdot 4H_2O$、2.8418g CH_4N_2S and 0.7g tetrabutylammonium bromide (TBAB) in a beaker containing 60 ml of deionized water, and stir with a magnetic stirrer for 30 minutes to form a uniform solution. Then transfer the solution to the reactor lining made of PTFE and place it in the stainless-steel reactor shell. The hydrothermal reactor was placed in a constant temperature blast drying oven and removed after 18 h of reaction at 210℃. The precipitate was collected by centrifugation and washed several times with deionized water and absolute ethanol, and the last wash precipitate was collected and dried in a vacuum drying oven for 24 h to obtain a 2H-MoS_2-TBAB powder sample.

Synthesis of anode material 2H-MoS_2-CTAB: the precursors are $(NH_4)_6Mo_7O_{24}\cdot 4H_2O$ (CASnumber:12054-85-2)、CH_4N_2S (CASnumber:6256-6) and Cetyltrimethylammonium bromide (CTAB) (CAS number:57-09-0) (the reagents used are purchased from the Reagent Network of Sinopharm Group and have not been further treated before use). Dissolve 1.4484g $(NH_4)_6Mo_7O_{24}\cdot 4H_2O$、2.8418g CH_4N_2S and 0.7g Cetyltrimethylammonium bromide (CTAB) in a beaker containing 60 ml of deionized water, and stir with a magnetic stirrer for 30 minutes to form a uniform solution. Then transfer the solution to the reactor lining made of PTFE and place it in the stainless-steel reactor shell. The hydrothermal reactor was placed in a constant temperature blast drying oven and removed after 18 h of reaction at 210℃. The precipitate was collected by centrifugation and washed several times with deionized water and absolute ethanol, and the last wash precipitate was collected and dried in a vacuum drying oven for 24 h to obtain a 2H-MoS2-CTAB powder sample.

Materials Characterizations

Phase, crystal structure, and microscopic morphology characterizations of samples were conducted by X-ray diffraction (XRD, PANalytical Empyrean) patterns with Cu K radiation, $\lambda = 0.15406$ nm, Field emission scanning electron microscope (FE-SEM, HiTACHI Regulus8220) and Energy-

dispersive X-ray spectroscopy (EDX, Oxford EDX, with INCA software), transmission electron microscope (TEM, JEOL JEM-2100) with configured EDX, X-ray photoelectron spectroscopy (XPS, AXIS SUPRA+ equipped with monochromatic Al Kα source). Raman spectroscopy was carried out by a LabRAMHR800 UV NIR spectrometer with 532 nm laser excitation. The surface area of the as-obtained sample was computed from the results of N_2 physisorption at 77 K (model: Micromeritics ASAP 2460 version 3.01) using the BET. Fourier-transform infrared (FT-IR) spectroscopy was tested using Thermo Scientific Nicolet iS5 spectrometer in the range of 4000-400cm^{-1}

Computational detail

DFT calculations were conducted through the Vienna ab initio Simulation Package (VASP) with the projector-augmented wave method. A generalized gradient approximation of the Perdew-Burke-Ernzerhof (PBE) functional was used as the exchange-correlation functional. The cutoff energy was set as 500 eV, and structure relaxation was performed until the convergence criteria of energy and force reached 1×10^{-5} eV and 0.03 eV Å^{-1}, respectively. A vacuum layer of 15 Å was constructed to eliminate interactions between periodic structures of surface models. The van der Waals (vdW) interaction was amended by the zero damping DFT-D3 method of Grimme. The adsorption energy (ΔE_{ads}) of Na adsorption on the surface is defined as

$$\Delta E_{ads} = E(*Na) - E(*) - E(Na)$$

where E(*Na) and E(*) are the total energy of surface systems with and without Na atoms, respectively, and E(Na) is the energy of an isolated Na atom. According to this definition, negative adsorption energy suggests that the adsorption process is exothermic and the adsorption system is thermodynamically stable. Contrarily, a positive value corresponds to endothermic and unstable adsorption. The migration barrier energies of Na in the interlayer of MoS_2 (001) are calculated by using the climbing image under the elastic band (CI-NEB) method. The calculations will be finished when the total energy difference is no higher than 1.0×10^{-6} eV per atom and maximum forces on each atom are within 0.03 eV/Å. The value of the migration energy barrier can be obtained by the following equation:

$$E_m=E_h-E_i \ (h>i)$$

of which the E_m is the migration energy barrier determined by the maximum value of the difference between E_h and E_i. E_h and E_i are the relative energies of transition states (h>i) referring to the initial state (seen as reference state with 0 eV in total energy).

Electrochemical tests

For the electrochemical tests of 2H-MoS_2, MoS_2-TBAB, and MoS_2-CTAB electrodes, the working electrodes in a three-electrode configuration were fabricated as followings: a mixture of active material (2H-MoS_2, MoS_2-TBAB, MoS_2-CTAB), polyvinylidene fluoride (PVDF) and Super P with a weight ratio of 8: 1: 1 was uniformly cast on carbon papers. The conductivity of the carbon paper (Toray, Japan) can reach ~ 17 240 S m^{-1}, The area of the working electrodes is ~1 cm^2, and the mass of loading of electrodes is 1~1.5 mg. Then the electrodes were dried in a vacuum oven at 60 °C for 24 hours. Platinum sheet as the counter electrode and Ag/AgCl (Saturated KCl) as the reference electrode. The gravimetric specific capacitance calculated from the galvanostatic charge-

discharge (GCD) curves is given by:

$$C = it/\Delta V \quad (1)$$

and it can be calculated from the cyclic voltammetry (CV) curves given by:

$$C = \frac{1}{\Delta V}\int\frac{j\,dV}{V} \quad (2)$$

Here, C is the specific capacitance (F g^{-1}), ΔV is the potential window (V), v is the scan rate (V s^{-1}), V is the potential (V), j is the current density (A g^{-1}), and t is time (s). All tests were performed using the lvium Vertex.C.EIS electrochemical workstation in 1 M Na_2SO_4 electrolyte.

To prepare the flexible electrodes, the slurry of the negative material MoS_2-CTAB and the positive material δ-MnO_2 is uniformly coated on the flexible carbon cloth, respectively. Then the carbon cloth coated with slurry is dried in a vacuum drying oven at 60°C for 24 hours. Subsequently, a MoS_2-CTAB flexible electrode and a δ-MnO_2 electrode which are coated with PVA-Glucose-Na_2SO_4 gel were assembled into a supercapacitor by sandwiching cellulose membrane as the separator between them. To achieve the best electrochemical performance of the MoS_2-CTAB//δ-MnO_2 flexible asymmetric supercapacitor (FASC) device, the charge balance is determined as $q^+ = q^-$. To achieve $q^+ = q^-$, the mass of the active material on the electrode definitely is:

$$\frac{m_+}{m_-} = \frac{C_{electrode-} \times \Delta v_-}{C_{electrode+} \times \Delta v_+} \quad (3)$$

The areal-specific capacitance of the device based on the area of the active material was calculated from charge-discharge curves according to the following equation:

$$C = \frac{I \times \Delta t}{S \times \Delta V} \quad (4)$$

where I is the constant discharge current (A); Δt is the time for a full discharge (s); S is the facing area of the active material on the two working electrodes (cm^2); and ΔV is the voltage drop on discharge (V). The areal energy densities (E = μWh cm^{-2}) and power densities (P = μW cm^{-2}) of the FASC device were calculated using the following equations:

$$E = 1 / (2 \times 3.6) \times C \times \Delta V^2 \quad (5)$$

$$P = 3600 \times E/\Delta t \quad (6)$$

Here, C is the areal-specific capacitance of the FASC device, ΔV is the potential window during the discharging process, Δt is the time for a full discharge of the device. The CV, GCD and cyclic stability tests of FASC devices assembled with MoS_2-CTAB and δ-MnO_2 as electrodes were performed using the lvium Vertex.C.EIS electrochemical work station.

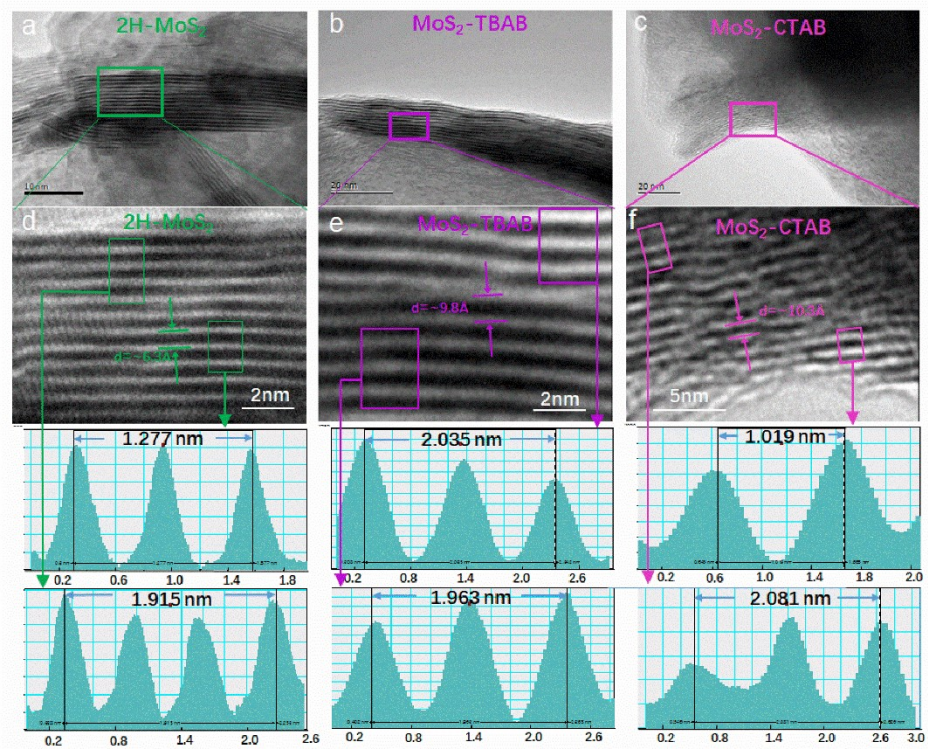

Fig. S1. HR-TEM images of (a) 2H-MoS_2, (b) MoS_2-TBAB and (c) MoS_2-CTAB. (e), (f) and (g) are the intensity changes of the line-scanning profile of the selected area enlarged HR-TEM which in panels a, b, and c, respectively.

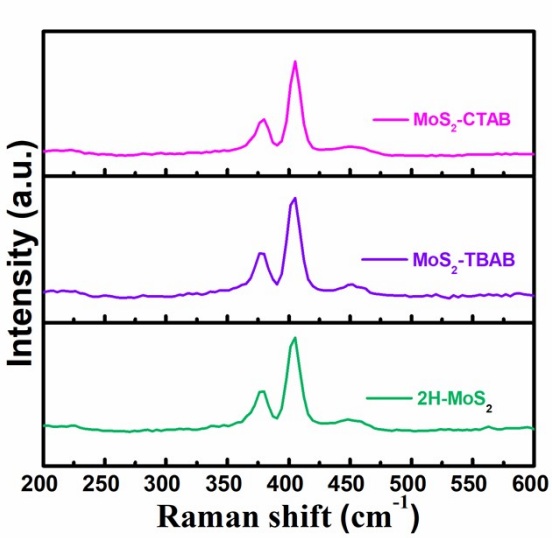

Fig. S2. Raman spectra of 2H-MoS_2、MoS_2-TBAB、MoS_2-CTAB.

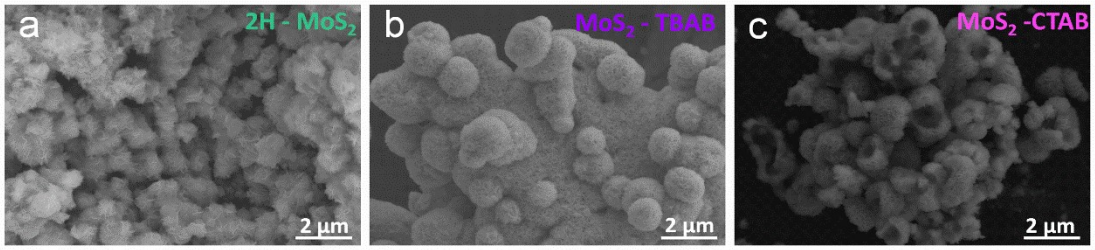

Fig. S3. SEM images of (a) 2H-MoS_2 (b) MoS_2-TBAB and (c) MoS_2-CTAB.

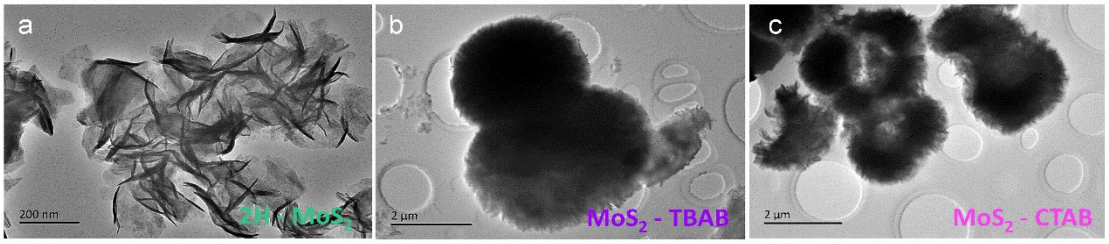

Fig. S4. TEM images of (a) 2H-MoS_2 (b) MoS_2-TBAB (c) MoS_2-CTAB.

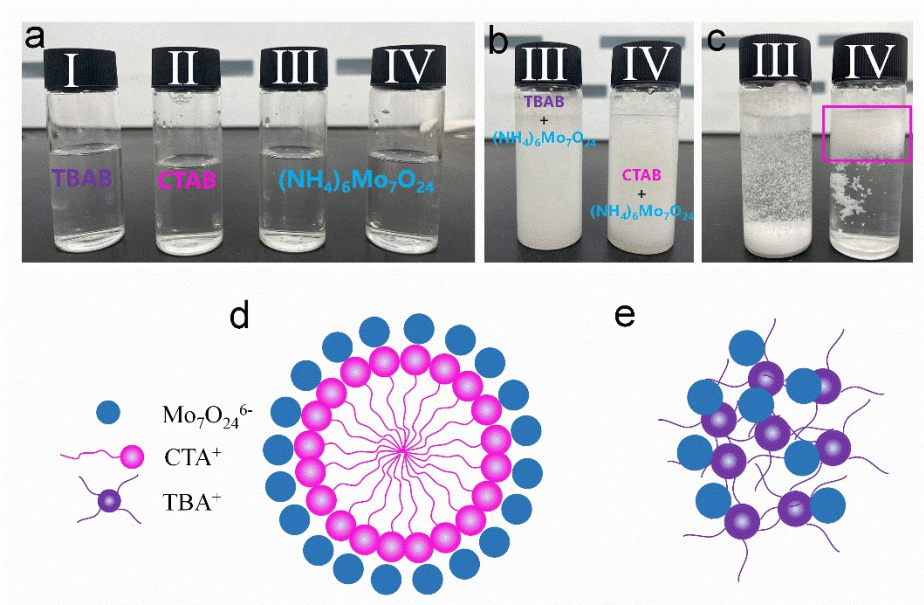

Fig. S5 (a) The pictures of solutions: TBAB (I), CTAB (II), $(NH_4)_6Mo_7O_{24}$ (III and IV), (b) the pictures of mixed solutions: TBAB+$(NH_4)_6Mo_7O_{24}$ (III), CTAB+$(NH_4)_6Mo_7O_{24}$ (IV), (c) the pictures of mixed solutions after standing for 20 minutes: TBAB+$(NH_4)_6Mo_7O_{24}$ (III), CTAB+$(NH_4)_6Mo_7O_{24}$ (IV), the diagrams of CTA^+ spherical micelle spectra (d) and TBA^+ amorphous micelles of (e).

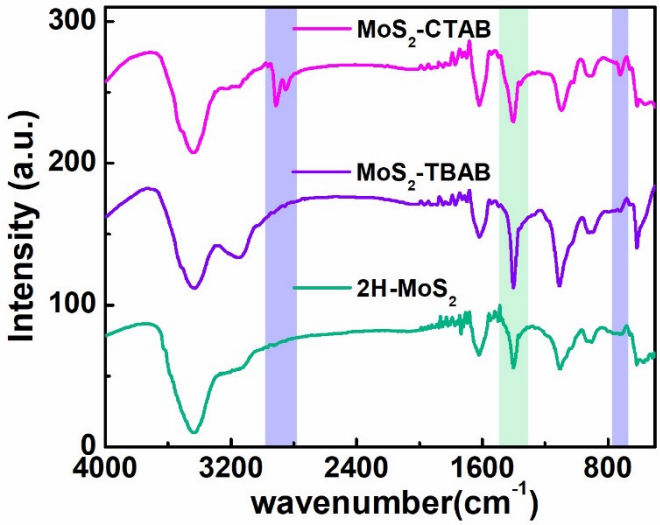

Fig. S6. FTIR spectra of 2H-MoS_2, MoS_2-TBAB and MoS_2-CTAB.

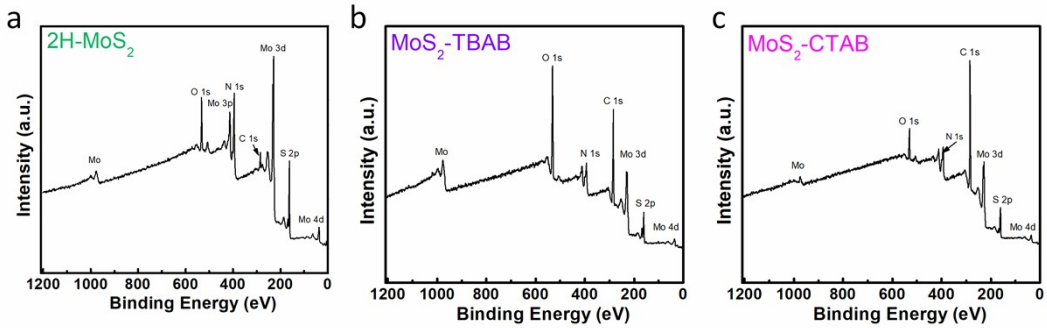

Fig. S7. XPS survey spectrum of (a) 2H-MoS_2 (b) MoS_2-TBAB and (c) MoS_2-CTAB.

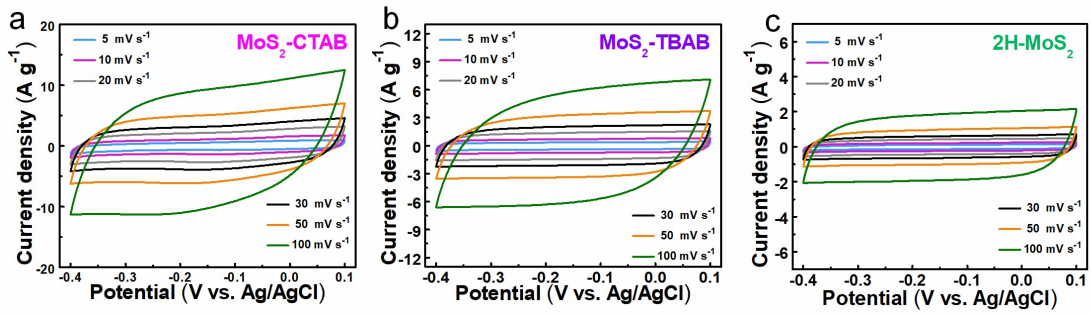

Fig. S8. (a-c) CV curves of MoS_2-CTAB, MoS_2-TBAB and 2H-MoS_2, respectively.

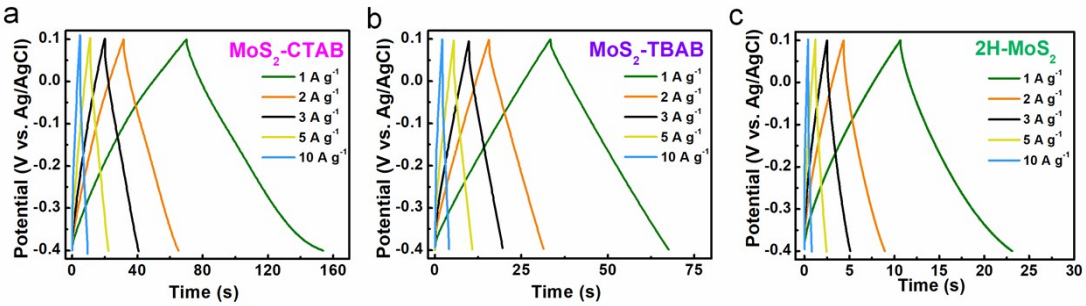

Fig. S9. (a-c) GCD curves of MoS_2-CTAB, MoS_2-TBAB and 2H-MoS_2, respectively.

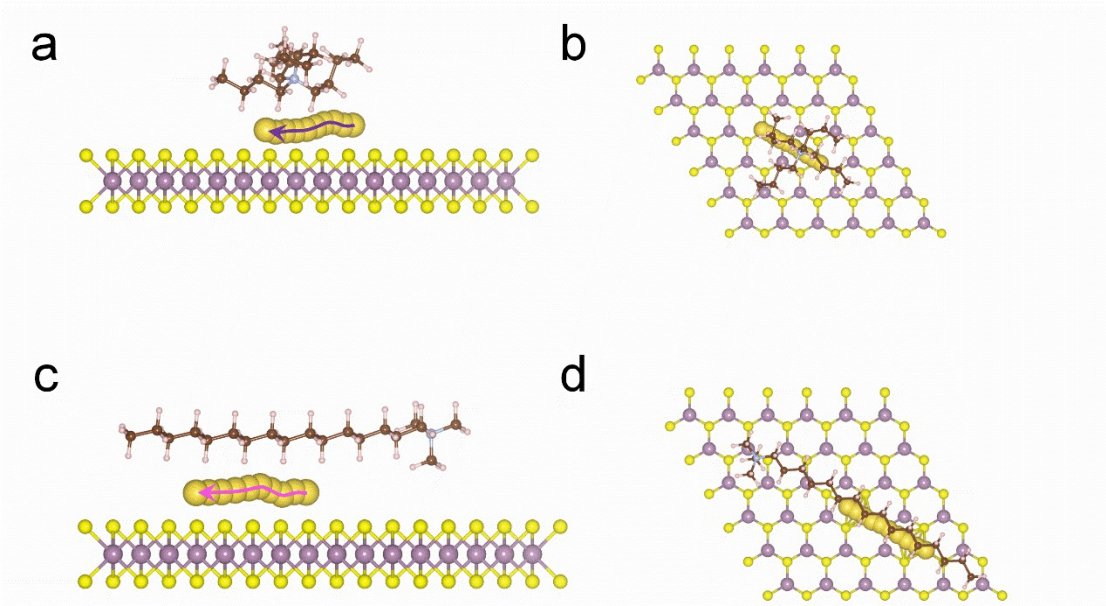

Fig. S10. (a) side view and (b) top view of Na diffusion on MoS_2-TBAB (The direction of the arrow is the migration direction of Na ion.). (c) side view and (d) top view of Na diffusion on MoS_2-CTAB (The direction of the arrow is the migration direction of Na ion.).

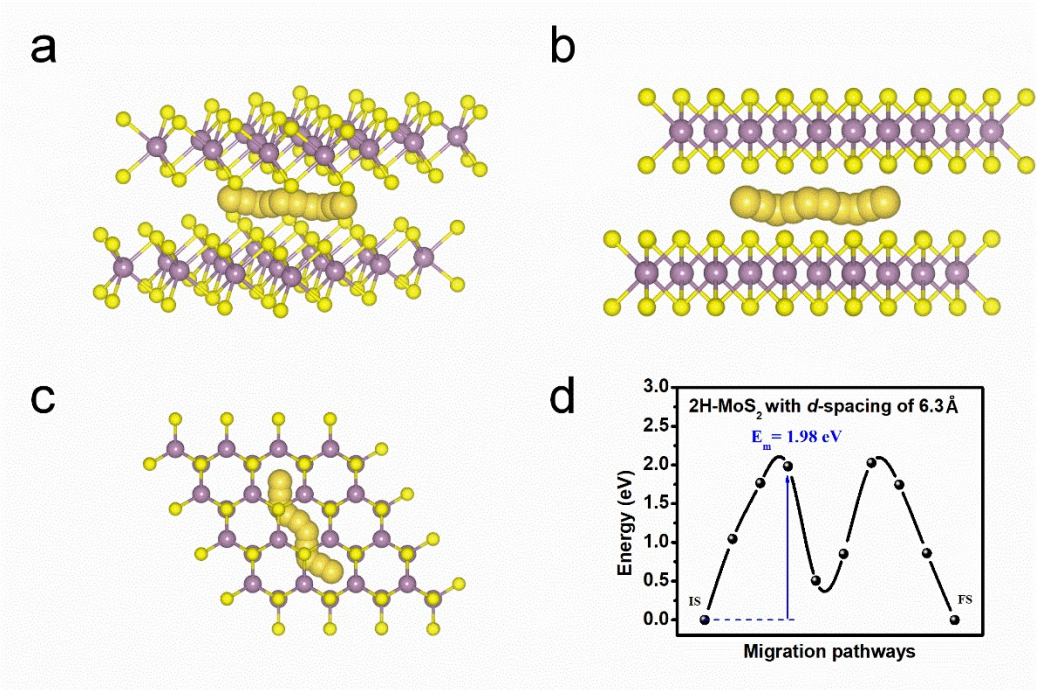

Fig. S11. (a-b) Side view and (c) top view of Na diffusion on 2H-MoS_2 with *d*-spacing of 6.3 Å (The direction of the arrow is the migration direction of Na ion.). (d) Diagram of diffusion barrier of Na on 2H-MoS_2 with *d*-spacing of 6.3 Å.

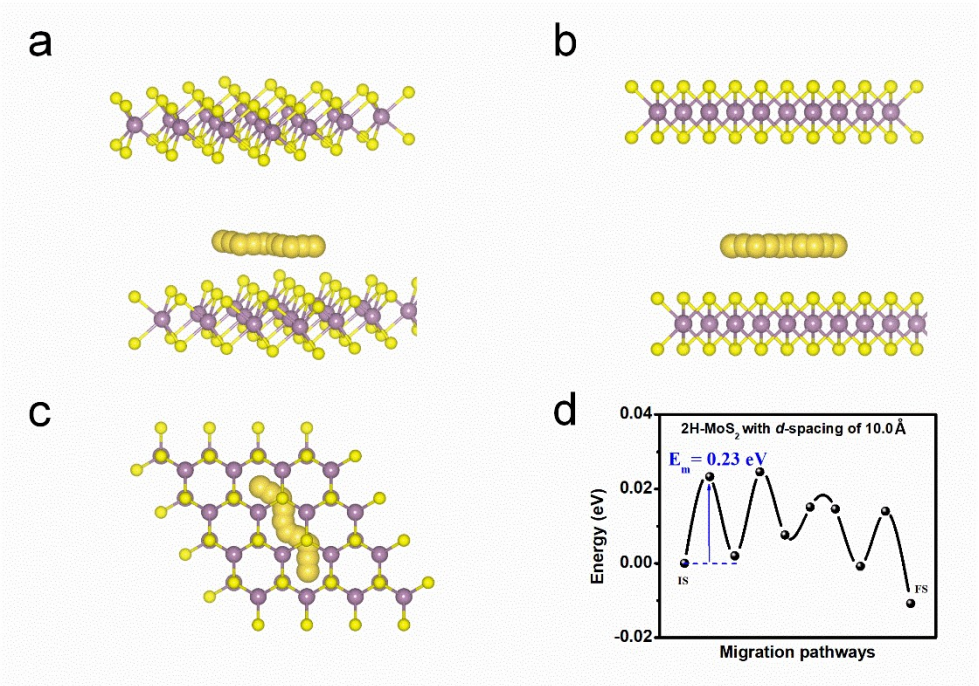

Fig. S12. (a-b) Side view and (c) top view of Na diffusion on 2H-MoS_2 with *d*-spacing of 10 Å (The direction of the arrow is the migration direction of Na ion.). (d) Diagram of diffusion barrier of Na on 2H-MoS_2 with *d*-spacing of 10 Å.

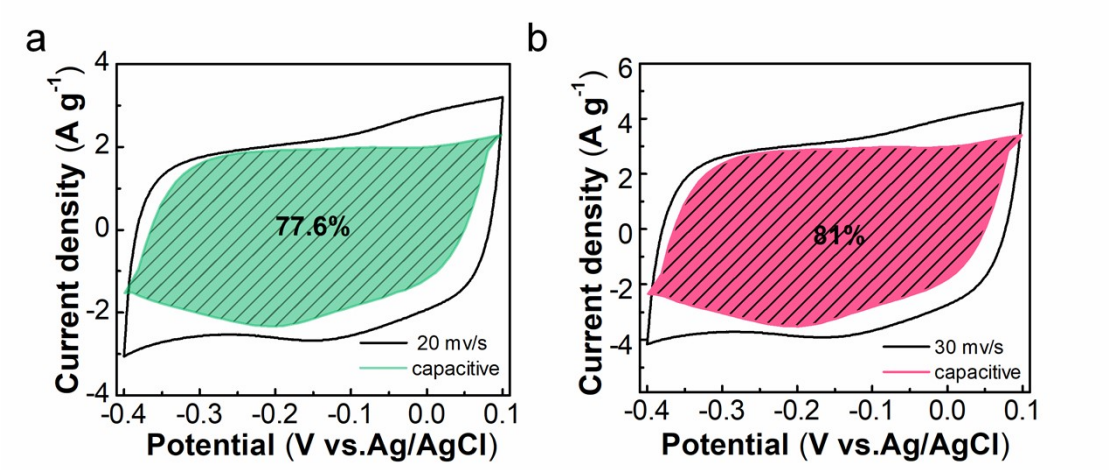

Fig. S13. The capacitive contribution of MoS_2-CTAB electrode at 20 and 30 mV s^{-1}.

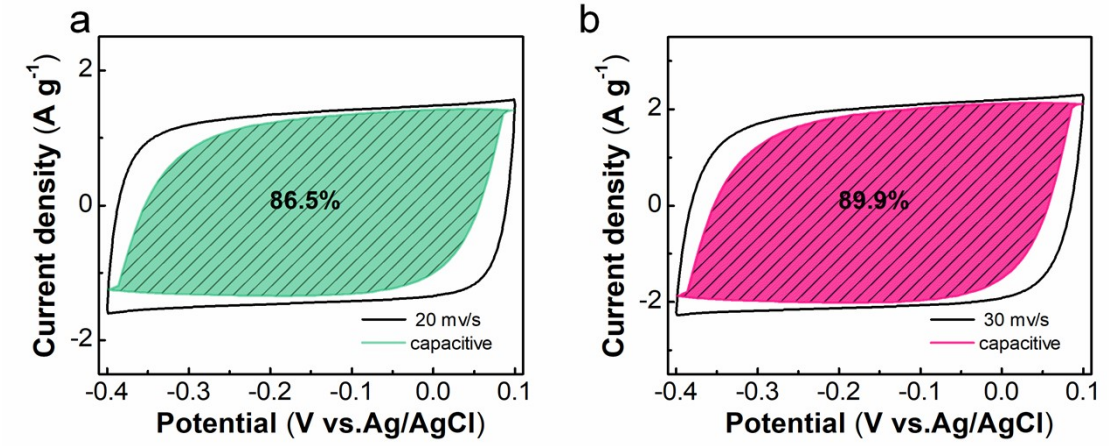

Fig. S14. The capacitive contribution of MoS_2-TBAB electrode at 20 and 30 mV s^{-1}

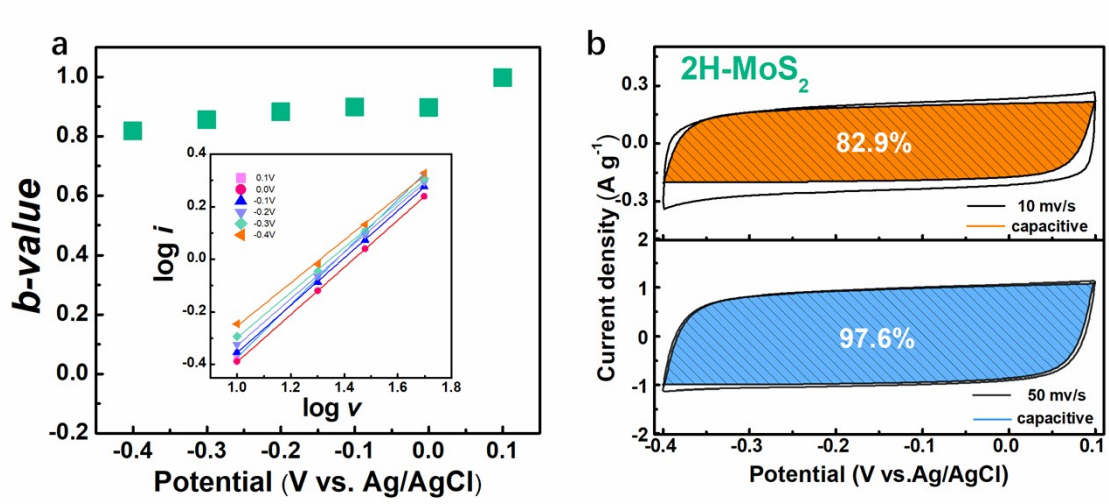

Fig. S15. (a)The *b* values for the 2H-MoS_2 electrode at a scanning speed of 10-50 mV s^{-1}; the inset shows the current response vs. the scan rate at different voltages. (b) CV partition analysis of 2H-MoS_2 shows the capacitive contribution to total current at 10 and 50 mV s^{-1} scan rates.

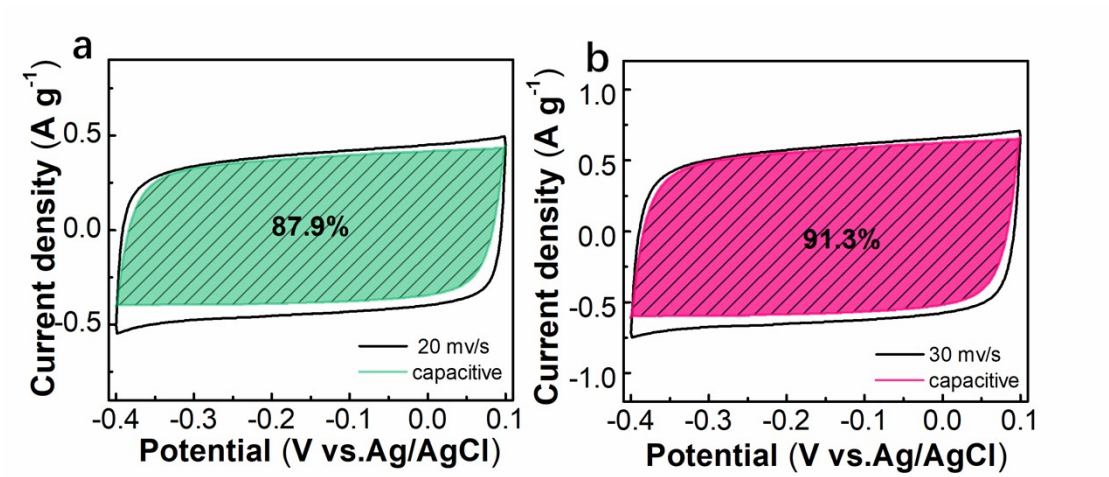

Fig. S16. The capacitive contribution of 2H-MoS_2 electrode at 20 and 30 mV s^{-1}

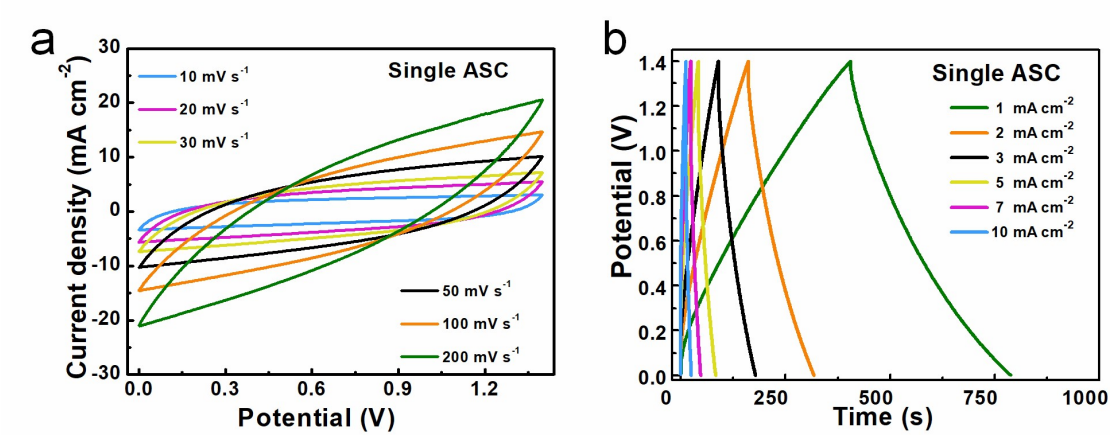

Fig. S17. (a) CV and (b) GCD curves of δ-MnO_2//MoS_2-CTAB single ASC device.

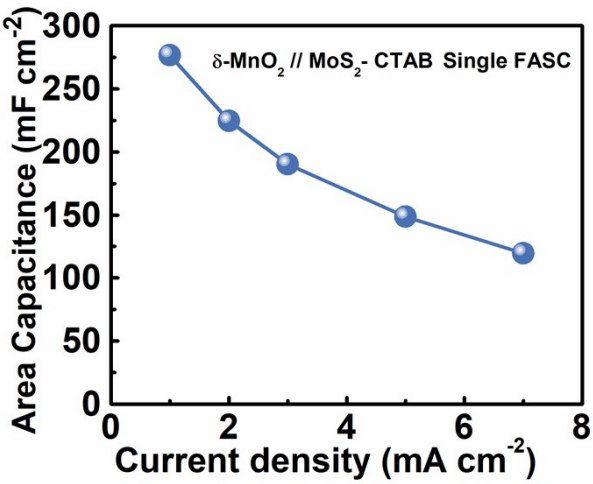

Fig. S18. Areal specific capacitance of δ-MnO_2//MoS_2-CTAB FASC device at a series of current density.

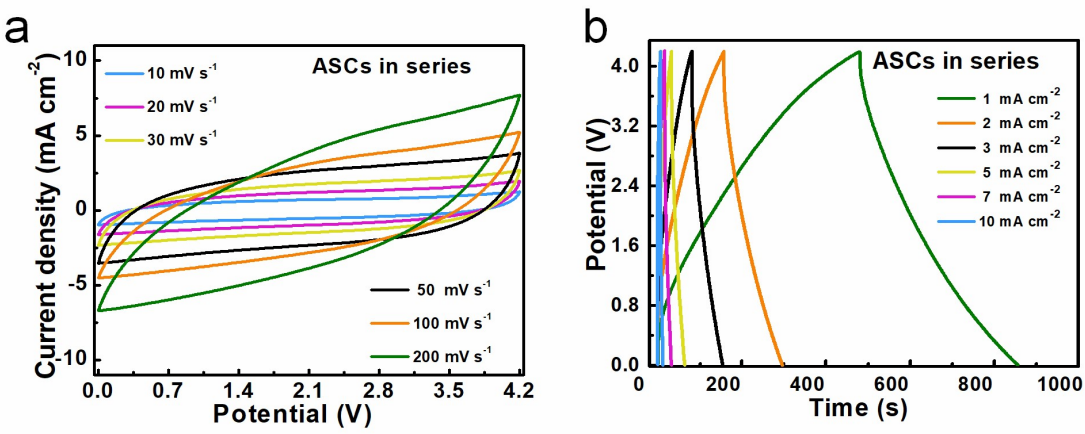

Fig. S19. (a) CV and (b) GCD curves of three δ-MnO_2//MoS_2-CTAB ASCs devices in series.

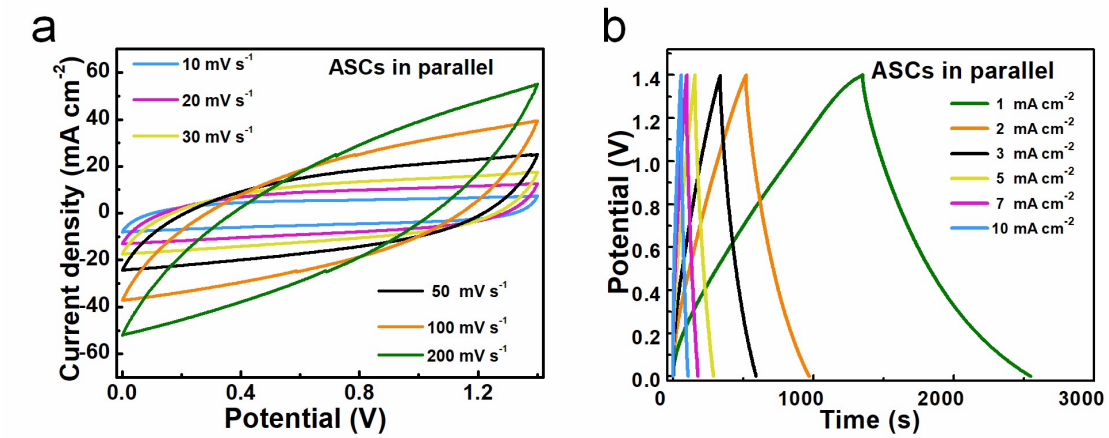

Fig. S20. (a) CV and (b) GCD curves of three δ-MnO_2//MoS_2-CTAB ASCs devices in parallel.

Table S1. Interplanar distance of 2H-MoS_2, MoS_2-TBAB and MoS_2-CTAB.

materials	Interplanar spacing (002) (Å)
2H-MoS_2	6.3
MoS_2-TBAB	9.8
MoS_2-CTAB	10.3

Table S2. Fitting results of XPS spectra of 2H-MoS_2 in Figure.

Mo 3d:

Peak Label	Position (eV)	FWHM (eV)	Area
+4	229.8	0.96	72669
+4	233.0	0.96	48837
S 2s	226.9	2.01	23480

N 1s：

Peak Label	Position (eV)	FWHM (eV)	Area
Mo 3p	395.7	2.54	136797
Pyridinic N	398.9	3.19	19785

Pyrrolic N	402.5	1.57	10018

S 2p:

Peak Label	Position (eV)	FWHM (eV)	Area
S^{2-} $2p_{3/2}$	162.7	0.81	63840
S^{2-} $2p_{1/2}$	163.8	0.81	31920

Table S3. Fitting results of XPS spectra of MoS_2-TBAB in Figure.

Mo 3d:

Peak Label	Position (eV)	FWHM (eV)	Area
+4	228.0	0.78	29820
+4	231.2	0.78	21416
+5	228.8	1.34	20923
+5	231.7	1.34	13243
+6	232.8	2.03	10934
+6	235.5	2.03	5210
S 2s	225.3	2.01	14360

N 1s：

Peak Label	Position (eV)	FWHM (eV)	Area
Mo 3p	394.1	2.28	32537
Pyridinic N	396.3	2.5	9654
Pyrrolic N	399.0	2.6	9314
N^+	401.2	1.86	4941

S 2p:

Peak Label	Position (eV)	FWHM (eV)	Area
S^{2-} $2p_{3/2}$	160.9	1	17158
S^{2-} $2p_{1/2}$	162.2	1	8740
S_2^{2-} $2p_{3/2}$	162.5	1	2943
S_2^{2-} $2p_{1/2}$	163.5	1	1766

Table S4. Fitting results of XPS spectra of MoS_2-CTAB in Figure.

Mo 3d:

Peak Label	Position (eV)	FWHM (eV)	Area
+4	228.0	0.69	26747
+4	231.2	0.69	19221
+5	228.8	1.64	21736
+5	231.7	1.64	17636
+6	231.8	2.16	20084
+6	235.5	2.16	9510
S 2s	225.3	2.15	13050

N 1s：

Peak Label	Position (eV)	FWHM (eV)	Area
Mo 3p	394.1	2.58	36643
Pyridinic N	396.3	2.5	7895
Pyrrolic N	399.0	3.15	7883
N^+	401.2	1.86	6500

S 2p:

Peak Label	Position (eV)	FWHM (eV)	Area
S^{2-} $2p_{3/2}$	160.9	1.14	16896
S^{2-} $2p_{1/2}$	162.2	1.14	9780
S_2^{2-} $2p_{3/2}$	162.6	1.78	4029
S_2^{2-} $2p_{1/2}$	163.6	1.78	2435

Table S5. Specific capacitances of 2H-MoS_2, MoS_2-TBAB, MoS_2-CTAB.

	1 A g^{-1}	**2 A g^{-1}**	**3A g^{-1}**	**5 A g^{-1}**	**10 A g^{-1}**	**15 A g^{-1}**
2H-MoS_2	25 F g^{-1}	19 F g^{-1}	17 F g^{-1}	14 F g^{-1}	11 F g^{-1}	9 F g^{-1}
MoS_2-TBAB	72 F g^{-1}	67 F g^{-1}	65 F g^{-1}	62 F g^{-1}	47 F g^{-1}	29 F g^{-1}
MoS_2-CTAB	166 F g^{-1}	142 F g^{-1}	133 F g^{-1}	124 F g^{-1}	118 F g^{-1}	116 F g^{-1}

Table S6. Adsorption energies of Na on MoS_2-TBAB and MoS_2-CTAB

Sample	*****	**Na**	***Na**
MoS_2-TBAB	-1091.51	-0.02205	-1092.92
MoS_2-CTAB	-1141.35	-0.02205	-1142.98

Table S7. Comparisons about the specific capacitance of Fitting results of MoS_2-CTAB electrode with those of MoS_2-based electrode materials reported recently.

Asymmetric devices	Energy and power density	Refs.
2H-MoS_2-CTAB//δ-MnO_2	75.3 μWh cm^{-2} at 700 μW cm^{-2} 40.4 μWh cm^{-2} at 3500 μW cm^{-2}	Our work
Cu $(OH)_2$/CPCC//AC/CC	0.49 μWh cm^{-2} at 600 μW cm^{-2}	*Chem. Eng. J.* **2019**, 371, 348.
NiO@MnO_2//Fe_2O_3	5.6 μWh cm^{-2} at 1680 μW cm^{-2} 9.62 μWh cm^{-2} at 28.9 μW cm^{-2}	*Chem. Eng. J.* **2018**, 347, 101.
Co-Al-LDH//$Ti_3C_2T_x$	10.8 μWh cm^{-2} at 250 μW cm^{-2}	*Nano Energy.* **2018**, 50, 479
CDCC//MnO_2/CDCC	30.1 μWh cm^{-2} at 150 μW cm^{-2} 5.8 μWh cm^{-2} at 7500 μW cm^{-2}	*Electrochim. Acta.* **2018**, 285, 262.
MnO_2//Ppy@MWCNT	12.16 μWh cm^{-2} at 136.8 μW cm^{-2}	*Small.* **2018**, 14, 1801809
FCNO/GF//CNR/GF	16.76 μWh cm^{-2} at 69.94 μW cm^{-2}	*Nano Res.* **2018**, 11, 1775-1786
Ti_3C_2/Fe-15%//MnO_2/CC	42 μWh cm^{-2} at 1600 μW cm^{-2} 20 μWh cm^{-2} at 8200 μW cm^{-2}	*Electrochim. Acta.* **2018**, 308, 1.
RGO/MnO_2//RGO	35.1 μWh cm^{-2} at 37.5 μW cm^{-2} 11.5 μWh cm^{-2} at 3800 μW cm^{-2}	*Adv. Mater.* **2013**, 25, 2809.
Poly-PNBTH//VACNT	23.5 μWh cm^{-2} at 14000 μW cm^{-2}	*ACS Appl. Polym. Mater* **2019**, 1, 1634.
P-TiON//MN	32.4 μWh cm^{-2} at 900 μW cm^{-2}	*Adv. Energy Mater.*

	21.9 μWh cm^{-2} at 4500 μW cm^{-2}	**2020**, 10, 2001873.
MnO_2/CNT//PI/CNT	36.4 μWh cm^{-2} at 780 μW cm^{-2}	*Carbon.*
	30.2 μWh cm^{-2} at 15600 μW cm^{-2}	**2017**, 125, 595-604.